ORIGINAL ARTICLE

Biocompatibility of calcitonin receptor fragment peptide-treated 3D-printed bone scaffolds: a muscle pouch implantation study

Vamiq M. Mustahsan[1,3,] Yanming Cai[3], David E. Komatsu[2], Imin Kao[3], Srinivas Pentyala[1,2]*

[1]Department of Anesthesiology, Stony Brook University Renaissance School of Medicine, Stony Brook, 11794, NY, United States of America,
[2]Department of Orthopaedics and Rehabilitation and Stony Brook University Renaissance School of Medicine, Stony Brook, 11794, NY, United States of America, [3]Department of Mechanical Engineering Stony Brook University College of Engineering and Applied Sciences, Stony Brook, 11794, NY, United States of America

ARTICLE INFO

Corresponding author:
Srinivas Pentyala
Anesthesiology, HSC L4, Room: 060,
Renaissance School of Medicine, Stony Brook,
NY, 11794-8480, United States of America.
Tel: +1 631-444-2974
Fax: +1 631-444-2907
Email: Srinivas.pentyala@stonybrook.edu

ABSTRACT

Background and Aim: Current synthetic bone graft substitutes (BGSs) in development are limited by high resorption, poor load-bearing properties, and stress shielding. These limitations inhibit BGS from complete biointegration. In this study, we developed calcitonin receptor fragment peptide (CRFP)-treated non-biodegradable MED610 scaffold, seeded with MC3T3 stem cells, and assessed their *in vivo* biocompatibility and biointegration.
Methods: Scaffolds were fabricated with Stratasys MED610 (MED610) material, seeded with Mus musculus calvaria cells (MC3T3), and osteogenesis was induced with CRFP after the cells reached confluency and generated bone matrix. Scaffolds with and without bone matrix were implanted in male mice following a muscle pouch implantation protocol. Post-extraction, imaging, staining, and mechanical compression testing was carried after 3 weeks of scaffold implantation in the muscle to measure the ectopic bone formation and compressive strength.
Results: The implanted scaffolds showed significantly higher ($P < 0.01$) calcium deposits in comparison to the untreated scaffolds. We also found significantly higher ($P < 0.001$) mineralization on the implanted scaffolds compared to scaffolds before implantation. The mechanical properties of the scaffolds did not vary significantly.
Conclusions: MED610 scaffolds treated with CRFP *in vivo* do not cause any adverse reaction when implanted in muscle and showed significant ectopic bone formation, indicating biocompatibility and bio-integration.
Relevance for Patients: This study will aid in developing biomimetic and biocompatible artificial bones for implantation.

1. Introduction

In many orthopedic surgical procedures, metallic implants are used to fill in the defects formed due to surgery or fracture [1-3]. Metallic implants are strong and are able to withstand the load experienced by the bone. However, metallic implants lead to stress shielding and, hence, weaken the surrounding bone [4]. Moreover, metallic implants are inert to bone growth and inhibit complete implant integration [5]. The alternative for metallic implants is biological implants *vis*, autografts and allografts [6]. Autografts are osteoconductive and promote bio integration of the implant as they are extracted from the subject's body [7]. They also have a lower rate of disease transmission in comparison to allografts. However, autografts have other complications *vis*, lower availability, excessive pain, and increased hospitalization cost due to extraction surgery [8,9]. Allografts exhibit reduced operating

cost and donor site complications, have a higher chance of antigen response and disease transmissibility [8-10]. Moreover, allografts are weaker in comparison to metallic implants leading to fractures and future revision surgeries [11,12].

Synthetic bone graft substitutes (BGSs) are being developed to overcome limitations in conventional metallic and biological implants [13]. Demineralized bone matrix (DBM), developed by removing all mineral content from bone, is the most common synthetic BGS [14,15]. However, the demineralization process makes it weak and reduces the load-bearing capacity of the implant [16-18]. Another class of implants is ceramic implants which are better load-bearing capability during implantation [19]. However, due to their high resorption rate, ceramic implants weaken with time and also form particulate matter, which may lead to an inflammatory response [20,21]. Ceramic implants are mostly used to fill in defects formed at non-load-bearing sites [22].

In recent years, three-dimensional (3D) printing technologies or additive manufacturing (AM) have facilitated the manufacturing of unique and complex shapes for a wide variety of materials. The flexibility to fabricate complex shapes and the ability to vary the design to manipulate the porosity of the BGS has led to 3D printing being used in the development of customized BGS [23-25]. These BGSs range from metallic and ceramic implants used in limb arthroplasties to polymer-based BGS, which are mostly in development stages to be introduced into mainstream applications [26-28]. The main issue with polymer-based BGS is that they are biodegradable and have a high resorption rate in the body leading to reduced strength with time and, hence, are not suitable for load-bearing sites in the body [20,29-31].

Earlier *in vitro* studies have shown that non-biodegradable materials such as ABS and Stratasys' MED610 have shown to produce long-term load-bearing implants, which are also osteoconductive and osteoinductive when pre-treated with bioactive reagents like calcitonin receptor fragment peptide (CRFP) [24,32-34]. We have earlier shown that CRFP has been found to be bioactive in differentiating stem cells into bone cells as well as enhance bone matrix production in *in vivo* studies [35,36]. In this study, we evaluate ectopic bone formation and biocompatibility of the non-biodegradable plastic MED610 scaffolds in a muscle pouch implantation model.

Ectopic bone refers to bone formation or ossification of tissue away from its typical origin *Vis*, in skin, fat, muscle, and other tissue environments [37]. Ectopic bone formation is usually used to study osteointegration in an *in vivo* setting by implanting the BGS outside its native environment. As the host's bone-forming cells are absent in this environment, ectopic bone formation is attributed to the influence of BGS [38-41]. The most common types of implantations are subcutaneous, kidney capsule, and muscle pouch implantations. Subcutaneous implantation may cause the implant to move under the skin of the rodent, causing complications, and a kidney capsule implantation requires a higher level of surgical skill to perform [37,42,43]. In this study, we adopted the muscle pouch implantation model in a mouse to

assess the biocompatibility of the 3D-printed MED610 scaffold, seeded with MC3T3 stem cells, and treated with CRFP.

2. Materials and Methods

2.1. Preparation of MED610 scaffolds

The trabecular bone structure was extracted from the L5 vertebrae of a skeletally mature male mouse through a computerized tomography (CT) scanning (μCT40, Scanco Medical, Wangen-Brüttisellen, Switzerland) at an isotropic voxel resolution of 10 μm. The CT imaging (DICOM files) were processed using InVesalius software (Renato Archer Information Technology Center, Sao Paolo, Brazil) to extract a 3D model. The 3D model is then imported and processed in Geomagic DesignX software (3D systems, Rock Hill, SC, USA) to extract the trabecular shape. Using this trabecular model, we design the planar scaffold region (1 mm thickness × 3 mm length × 3 mm height). We also designed two cylindrical plates (3 mm diameter × 1 mm height) on the top and bottom of this planar region to facilitate compression studies. The scaffold's dimensions were chosen to fit in the lower extremity muscles of a mouse. The designed scaffolds were fabricated using MED610 material on a polyjet 3D printer (Objet 30 Prime; 16-μm resolution, Stratasys, Eden Prairie, MN, USA). The workflow of the design of MED610 scaffolds is presented in Figure 1.

The MED610 scaffolds were, then, washed with deionized water and sterilized in an autoclave oven at 132°C for 4 min as per the manufacturer's recommendation. The sterilized scaffolds were air-dried in a sterile cell-culture hood for 60 min. These scaffolds were, then, attached to the bottom surface of the cell culture plate using sterile grease to prevent them from floating in the cell culture media. MC3T3-E1 stem cells extracted from the C3 vertebra of a mouse were seeded with a cell density of 1×10^3 cells per chamber onto the scaffold surface [44]. The cell culture media (MEMα supplement with 5% fetal bovine serum and 1% penicillin/streptomycin) was changed every 3 days until 80% cell confluency was reached.

Osteogenesis was induced by adding 4 mM β-glycerol phosphate (G6P), 0.05 μg/μL ascorbic acid (AA), and 2 μM CRFP [45,46]. The cells were cultured for 3 more weeks with osteogenic reagents, with the media being changed every 3 days. In 3 weeks, the stem cells differentiate into bone cells and produce a bone matrix on the surface of the scaffolds. The scaffolds were, then, decellularized with 0.1% sodium dodecyl sulfate (SDS) solution for 5 min, washed in Dulbecco's phosphate buffer saline (DPBS) 2 times, and stored in DPBS.

2.2. Experimental design of muscle plant implantation in mice

Fourteen male C57BL/6J strain male mice of 10 – 12 week old (Charles River Laboratories, Sao Paolo, Brazil) were purchased and housed individually as males are known to fight if co-housed and tend to nibble at the healing incisions of their cage mates. The acclimatization period was 9 days at 12 h light/dark cycles, and the animals had libitum access to standard mouse chow and water. These conditions were maintained throughout the experiment. After acclimatization, mice were weighed and

randomized into two experimental groups (*n* = 7): (1) Untreated scaffolds and (2) decellularized scaffolds. Decellularized scaffolds were prepared using the protocol explained in section 2.1. A set of untreated scaffolds which were exposed to the same reagents as decellularized scaffolds were also prepared, except that they do not have any stem cells seeded onto the surface.

2.3. Surgical protocol

For implantation, animals were anesthetized with isoflurane (2% induction and 1.5% maintenance) (Covetrus, Portland, ME, USA). Eye lubrication (Optixcare; Aventix, Burlington, Ontario, Canada) was applied, and the mice were prepared for the surgery by shaving the left hind limb and sterilizing the surgical site with betadine and ethanol (Sigma-Aldrich, Saint-Louis, MO, USA). A 10-mm longitudinal incision parallel to the posterior femur was created. Using a blunt dissection to prevent muscle damage, a 5-mm deep intramuscular pouch was then shaped, taking precautions not to expose the periosteum. A scaffold was, then,

sterilized in 70% ethanol and implanted into the muscle pouch, and the fascia over the muscle was sutured with resorbable sutures (Ethicon, Raritan, NJ, USA) to close the muscle wound. The skin incision was closed using non-resorbable sutures (Ethicon), and topical antibiotics were applied. Buprenorphine (0.1 mg/kg) analgesia (Buprenex, Indivior, North Chesterfield, VA, USA) was administered immediately following surgery and twice daily thereafter until it was judged to be no longer necessary. The skin sutures were removed 10 – 14 days after surgery. The workflow of the surgery is illustrated in Figure 2.

The animals were monitored every day for the first 3 days and weekly thereafter. Movement around the cage and activity was observed to assess the weight-bearing on the lower extremity. The incision area was assessed for incision and quality of sutures. Grooming, vocalization, and weight loss were checked as indicators of distress. The exclusion criteria were if the animal is experiencing dehiscence, infection, pain, or distress that cannot be treated or if the animal is experiencing more than 15% weight loss.
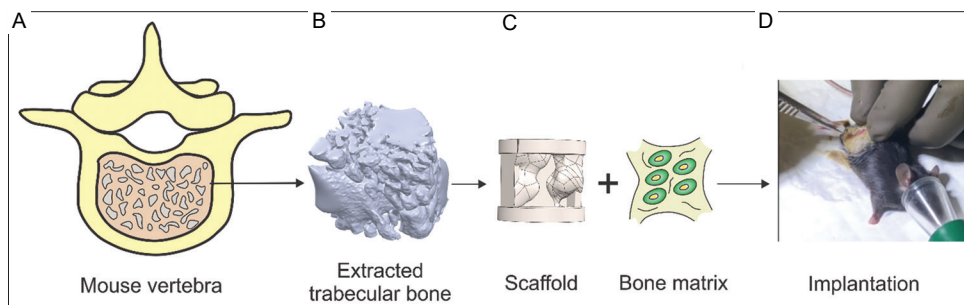

Figure 1. (A) The cross-section of a mouse vertebra with cortical bone (yellow) and trabecular bone (brown); (B) Trabecular bone extracted from μ-computed tomography scan of the vertebra; (C) MED610 scaffold designed from the extracted trabecular bone seeded with bone cells on its surface; and (D) Scaffold being implanted into the thigh muscle of a mouse.
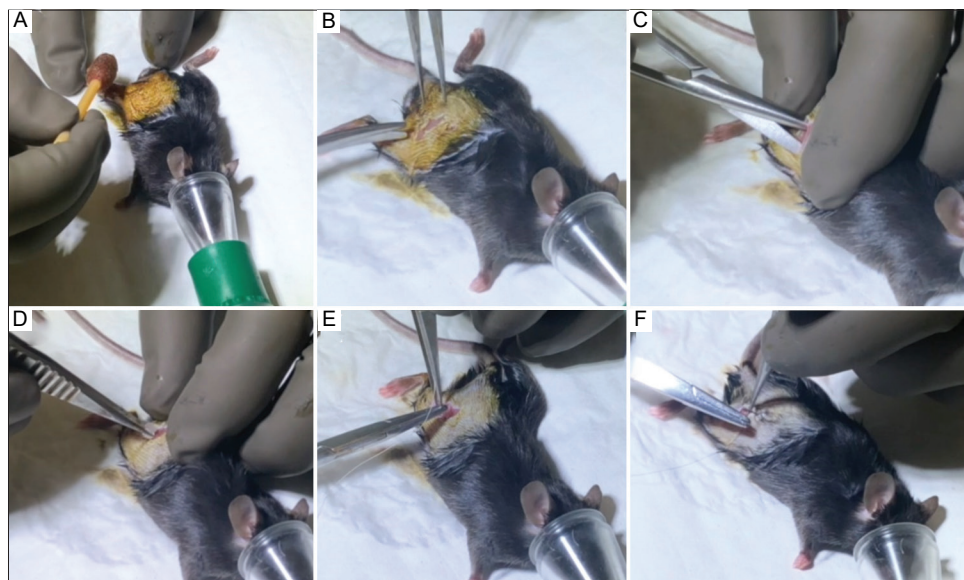

Figure 2. (A) Preparing the surgical site by scrubbing the shaved skin with Betadine: (B) Longitudinal incision made along the thigh; (C) Blunt dissection being carried out to create a muscle pouch without exposing the periosteum; (D) Implant placed in the muscle pouch; (E) muscle pouch was closed with resorbable sutures; and (F) The skin incision was sutured with non-resorbable sutures.

2.4. Extraction and post-operative testing

After 3 weeks, the mice were euthanized with a lethal dose of isoflurane, and the scaffolds were extracted for post-operative mechanical and staining studies. The scaffolds extracted from the animals were fixed in 4% formaldehyde solution for 24 h and washed and stored in DPBS for post-operative studies. The previous studies have shown that pre-coating the BGS with CRFP leads to enhanced osteoinduction which results in the deposition of more bone matrix, contributing to improving the load-bearing capacity, that is, the compressive strength of the BGS. Therefore, we performed unconstrained mechanical compressive testing (MTEST Quattro, Admet, Norwood, MA, USA) on four sets of MED610 scaffolds (Table 1). For this purpose, the force was applied in the direction of the axis of the scaffold, as illustrated in Figure 3B. The speed of compression was set to 5 mm/min based on the ISO 604, international standards for plastics [47]. Stiffness (k), maximum compressive strength (σ_M), and compressive modulus (E_C) in the central axis were evaluated. Thereafter, Shapiro–Wilk test was carried out for the compressive test results of each type of scaffold to assess the normality of the data before carrying out the statistical analysis. A one-way analysis of variance (ANOVA) test at a significance level of 0.0083 (Bonferroni correction) was performed to compare the different strength characteristics of the various scaffolds.

Post-compression tests, scanning electron microscopy (SEM) imaging (10.0 K × magnification at electron high-tension voltage of 3.0 kV) was performed to observe the surface of the different groups of scaffolds. Thereafter, staining studies with 2% Alizarin red to validate calcium deposits and Von Kossa staining to validate mineralization on the BGS surface were conducted. The Alizarin red-stained scaffolds were imaged using a confocal microscope (LSM-510; Zeiss, Oberkochen, Germany). We followed up these studies with histological studies using Nuclear Fast Red (Kernechtrot) staining for calcium and were imaged using a confocal microscope (upright DM 6000; Leica Microsystems, Wetzlar, Germany). In these staining studies, ten regions of interest (ROI) (0.7 mm × 0.7 mm) were identified for analysis in each image of the stained scaffold. For Alizarin red staining and Nuclear Fast Red staining, each ROI image was processed to isolate the red-colored pixel intensity map from the Red-Blue-Green (RGB) color image. This red color intensity map then is normalized such that "0" is the least red (100% white) and "1" is the value for the highest red value (100% red). Then, the average of this normalized intensity pixel map was calculated to represent the measure of the red intensity of the ROI. The higher red intensity measure indicates more red spots on the ROI (representing higher deposition of calcium deposits). In the case of Von Kossa staining, the RGB color image was converted to a grayscale image and normalize the grayscale image such that the "0" value refers to the brightest pixel (100% white) and "1" value refers to the darkest

Table 1. Types of MED610 scaffolds.

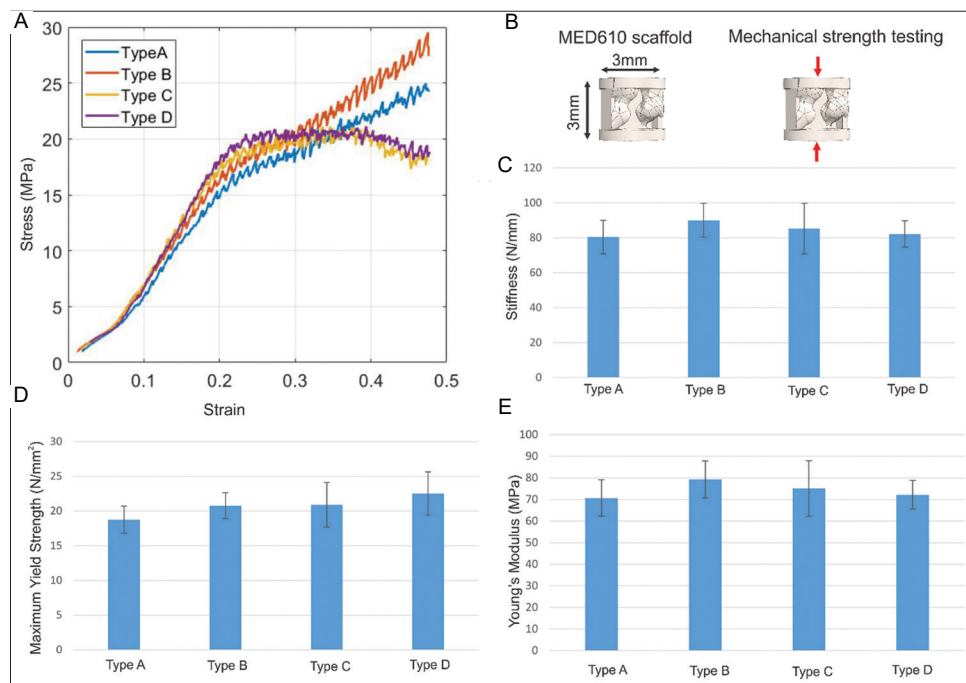| Type	Protocol
A	Untreated scaffolds
B	Decellularized scaffolds
C	Implanted untreated scaffolds
D	Implanted decellularized scaffolds

Figure 3. (A) Stress-strain curve of the four types of scaffolds and (B) the dimensions of the MED610 scaffolds and the direction of mechanical compression testing. Plots of stiffness (C), maximum compressive strength (D), and compressive modulus (E) for the four types of scaffolds (n = 7) in Table 1. Error bars represent standard deviation.

pixel (100% black). The darker spots on the image represent the higher mineralization deposition on the ROI. One-way ANOVA analysis at a significance level of 0.0083 (Bonferroni Correction) was performed to compare unseeded scaffolds with decellularized scaffolds.

3. Results

3.1. Mechanical testing for the strength of the scaffolds

In the implantation study, the animals did not show any signs of infection or prolonged distress due to implantation throughout the duration of the study, and by the 10th day, they were able to regain complete range of motion and were able to walk/run without any signs of pain or distress. All animals maintained their weight by the end of the study and did not trigger any exclusion criteria.

In the mechanical testing of the four types of scaffolds listed in Table 1, the data followed normal distribution using Shapiro–Wilk test. Thereafter, the one-way ANOVA test showed no significant difference in stiffness (k), maximum compressive strength (σ_M), and compressive modulus (E_C). However, on plotting the stress-strain data shown in Figure 3A from the stress-strain curves, it was noted that the decellularized scaffolds with bone matrix (type B and D) show superior trends for maximum yield strength (σ_M) in comparison to untreated scaffolds without bone matrix (type A and C). These findings follow our earlier reported results [24]. The strength characteristics (k, σ_M, and E_C) of all types of scaffolds are illustrated in Figure 3.

The SEM study of the scaffolds' surfaces is illustrated in Figure 4. The surface of the scaffolds shows deposition of bone matrix in the type B scaffolds, in comparison to type A scaffolds. When these scaffolds are implanted, type D scaffolds show more deposition of organic material, indicating a higher level of biointegration in comparison to type C scaffolds.

For the Alizarin red staining study for validating calcium deposits on the scaffolds' surfaces, the one-way ANOVA analysis showed a significant increase in calcium deposits from type A (untreated scaffolds) to implanted scaffolds, that is, Type C ($P = 0.005$) and Type D ($P = 0.0027$). All other comparisons between scaffolds were not statistically significant. These results are represented in Figure 5A.

For the Von Kossa staining study to validate mineralization on the surface of the scaffolds, the one-way ANOVA analysis showed that Type B and Type D (demineralized) scaffolds showed a significantly higher mineralization on the scaffold surface compared to Type A and Type C (untreated) scaffolds ($P < 0.001$ for all significant comparisons). The comparisons are illustrated in Figure 5B. The confocal microscopy results with Nuclear Fast Red staining shows a significantly higher calcium deposition in demineralized scaffolds (Types B and D) compared to untreated scaffolds (Types A and C) in the one-way ANOVA analysis ($P < 0.001$), as illustrated in Figure 6.

4. Discussion

In this study, we developed non-biodegradable BGS from Stratasys MED610 material for testing the biocompatibility of artificial bone in an *in vivo* environment. The BGS was fabricated using polyjet 3D printing to achieve a high-resolution surface that
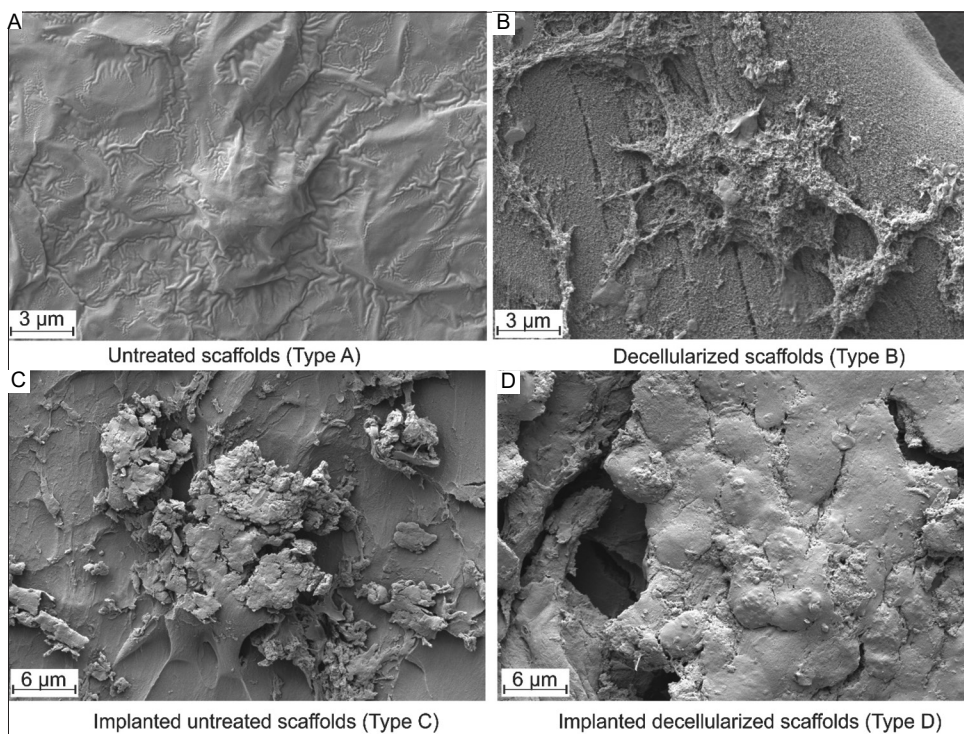

Figure 4. (A-D) Scanning electron microscopy images of different scaffolds taken at 2.0K × magnification showing the deposition of organic material on the scaffold surfaces.
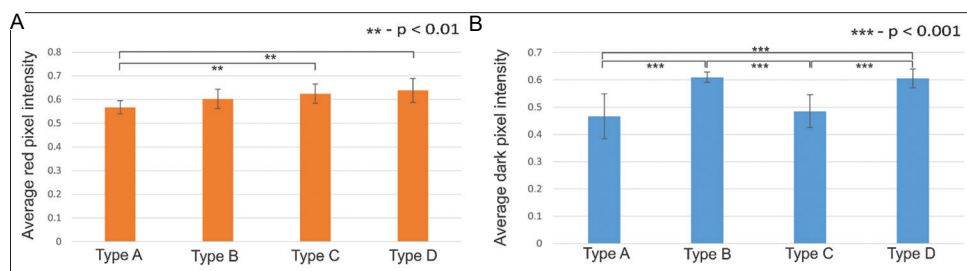
Figure 5. (A and B) Results of mean values of average red pixel intensity (orange) in Alizarin red staining for calcium deposits and mean value for average dark pixel intensity in Von Kossa staining (blue) for mineralization on scaffolds' surface (*n* = 10). Error bars represent the standard deviation.
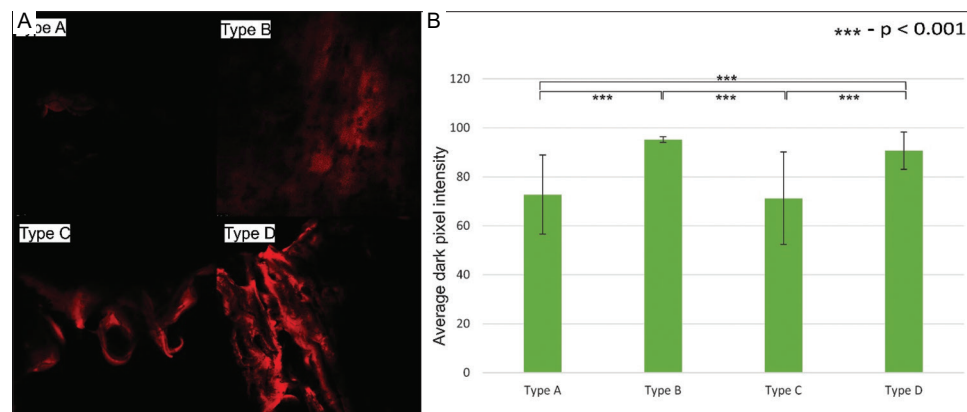

Figure 6. (A) Confocal microscopy images if the different scaffolds with nuclear fast red staining showing calcium deposition in different scaffolds. (B) Results of mean values of average red pixel intensity (green) in nuclear fast red staining for calcium deposits (*n* = 12). Error bars represent the standard deviation.

mimics the trabecular structure of the bone [33,48]. The previous studies suggest that most of the plastic (PLA/PLC) and ceramic (TCP) BGS being developed today show reduced strength over time and cannot consistently bare the stresses applied to the bone leading to them only being used in non-loadbearing sites [20,49]. This is due to the high resorption rate of the BGS. Our scaffolds (BGS) maintain their structural integrity and strength as they are non-biodegradable and show high potential as BGS in loadbearing areas.

In our muscle pouch implantation study, our BGS exhibited good biocompatibility, as the animals were able to accept the BGS and did not show any inflammatory response near the incision or internally [50]. By the 10th day after implantation, all animals were behaving normally without any distress and complete load bearing.

In SEM imaging study, we find that the decellularized scaffolds, when implanted, have a higher deposition of organic material on the scaffold surface in comparison to the untreated scaffolds (Figure 4). Following up with the staining studies with Alizarin red, Nuclear Fast Red, and Von Kossa staining, we find that the implanted decellularized scaffolds show a significantly higher level of calcium deposits and mineralization. We also see that there is a significantly higher level of calcium deposit on the implanted scaffolds in comparison to the untreated scaffolds. This is an indication of ectopic bone formation on the scaffold surface and bio integration on implantation.

Earlier studies reported that the strength of the BGS increases when the bone matrix is deposited on the scaffold surface [24,33]. In our mechanical strength studies, we find no significant increase in decellularized scaffolds compared to untreated scaffolds. However, the results suggest that the maximum yield strength follows similar trends to that of the *in vitro* studies in the literature, where scaffolds with bone matrix perform better than scaffolds without bone matrix [24,33,51,52].

One of the limitations of this study was the size of the scaffolds (3mm diameter × 3mm height). Due to the small size of the animals, the aim was only to observe the ectopic bone formation and biocompatibility of the MED610 material. In future, these studies will be followed up by a segmental defect model in either rats or rabbits so that the biointegration of these scaffolds with the surrounding bone can be studied and evaluate how BGS can maintain the strength at a load-bearing site.

Another limitation of this study was that we did not mimic any specific bone as done in studies by others [33,53], except taking the trabecular structure model. Despite considerable progress in the field of artificial bone development using materials like natural polymers[54-59], synthetic polymers[60-62], biocermaic and bioglass[63-66], metal[67-69], and composites[70-74], an ideal all-purpose material for scaffold-guided bone regeneration is currently not available[75]. In future biointegration studies, we plan to design the scaffolds precisely in the shape of the bone that is to be replaced to achieve complete integration structurally

and biologically. Many iterations need to be done on the design side to achieve the balance between having the ideal porosity to facilitate the bone growth and providing the structural strength to the affected bone.

5. Conclusions

We successfully demonstrated that our MED610 3D-printed scaffolds are suitable for implantation as they are biocompatible and do not cause any adverse reaction when implanted. We also found that the CRFP-coated MED610 scaffolds generate more ectopic bone growth when implanted and contribute to bio-integration.

Acknowledgments

The authors gratefully acknowledge the support provided by the Department of Anesthesiology, Renaissance School of Medicine, Stony Brook, NY.

Conflicts of Interst

The authors declare that there are no conflicts of interest.

Ethics Approval and Consent to Participate

No human subjects were involved in this study. All procedures involving animals were reviewed and approved by the Institutional Animal Care and Use Committee of Stony Brook University (IACUC protocol number: 1503487).

Consent for Publication

Not applicable.

References

[1] Sohn HS, Oh JK. Review of Bone Graft and Bone Substitutes with an Emphasis on Fracture Surgeries. Biomater Res 2019;23:9.

[2] Myers GJ, Abudu AT, Carter SR, Tillman RM, Grimer RJ. Endoprosthetic Replacement of the Distal Femur for Bone Tumours: Long-term Results. J Bone Joint Surg Br 2007;89:521-6.

[3] Plotz W, Rechl H, Burgkart R, Messmer C, Schelter R, Hipp E, et al. Limb Salvage with Tumor Endoprostheses for Malignant Tumors of the Knee. Clin Orthop Relat Res 2002;405:207-15.

[4] Engh CA, Bobyn JD, Glassman AH. Porous-coated Hip Replacement. The Factors Governing Bone Ingrowth, Stress Shielding, and Clinical Results. J Bone Joint Surg Br 1987;69:45-55.

[5] Epari DR, Taylor WR, Heller MO, Duda GN. Mechanical Conditions in the Initial Phase of Bone Healing. Clin Biomech (Bristol, Avon) 2006;21:646-55.

[6] De Long WG Jr., Einhorn TA, Koval K, McKee M, Smith W, Sanders R, et al. Bone Grafts and Bone Graft Substitutes in Orthopaedic Trauma Surgery. A Critical Analysis. J Bone Joint Surg Am 2007;89:649-58.

[7] Finkemeier CG. Bone-grafting and Bone-graft Substitutes. J Bone Joint Surg Am 2002;84:454-64.

[8] Tomford WW. Transmission of Disease through Transplantation of Musculoskeletal Allografts. J Bone Joint Surg Am 1995;77:1742-54.

[9] Buck BE, Malinin TI, Brown MD. Bone Transplantation and Human Immunodeficiency Virus. An Estimate of Risk of Acquired Immunodeficiency Syndrome (AIDS). Clin Orthop Relat Res 1989;240:129-36.

[10] Boyce T, Edwards J, Scarborough N. Allograft Bone. The Influence of Processing on Safety and Performance. Orthop Clin North Am 1999;30:571-81.

[11] Mroz TE, Joyce MJ, Steinmetz MP, Lieberman IH, Wang JC. Musculoskeletal Allograft Risks and Recalls in the United States. J Am Acad Orthop Surg 2008;16: 559-65.

[12] Ullmark G, Obrant KJ. Histology of Impacted Bone-graft Incorporation. J Arthroplasty 2002;17:150-7.

[13] Fernandez de Grado G, Keller L, Idoux-Gillet Y, Wagner Q, Musset AM, Benkirane-Jessel N, et al. Bone Substitutes: A review of their Characteristics, Clinical Use, and Perspectives for Large Bone Defects Management. J Tissue Eng 2018;9:2 041731418776819.

[14] Wang JC, Alanay A, Mark D, Kanim LE, Campbell PA, Dawson EG, et al. A Comparison of Commercially Available Demineralized Bone Matrix for Spinal Fusion. Eur Spine J 2007;16:1233-40.

[15] Gruskin E, Doll BA, Futrell FW, Schmitz JP, Hollinger JO. Demineralized Bone Matrix in Bone Repair: History and Use. Adv Drug Deliv Rev 2012;64:1063-77.

[16] Campana V, Milano G, Pagano E, Barba M, Cicione C, Salonna G, et al. Bone Substitutes in Orthopaedic Surgery: From Basic Science to Clinical Practice. J Mater Sci Mater Med 2014;25:2445-61.

[17] Russell N, Walsh WR, Lovric V, Kim P, Chen JH, Larson MJ, et al. In-vivo Performance of Seven Commercially Available Demineralized Bone Matrix Fiber and Putty Products in a Rat Posterolateral Fusion Model. Front Surg 2020;7:10.

[18] Chung HJ, Hur JW, Ryu KS, Kim JS, Seong JH. Surgical Outcomes of Anterior Cervical Fusion Using Deminaralized Bone Matrix as Stand-Alone Graft Material: Single Arm, Pilot Study. Korean J Spine 2016;13:114-9.

[19] Saikia KC, Bhattacharya TD, Bhuyan SK, Talukdar DJ, Saikia SP, Jitesh P. Calcium Phosphate Ceramics as Bone Graft Substitutes in Filling Bone Tumor Defects. Indian J Orthop 2008;42:169-72.

[20] Hing KA, Wilson LF, Buckland T. Comparative Performance of Three Ceramic Bone Graft Substitutes. Spine J 2007;7:475-90.

[21] Flatley TJ, Lynch KL, Benson M. Tissue Response to

Implants of Calcium Phosphate Ceramic in the Rabbit Spine. Clin Orthop Relat Res 1983;260:246-52.

[22] Koshino T, Murase T, Takagi T, Saito T. New Bone Formation around Porous Hydroxyapatite Wedge Implanted in Opening Wedge High tibial osteotomy in patients with osteoarthritis. Biomaterials 2001;22:1579-82.

[23] Bose S, Vahabzadeh S, Bandyopadhyay A. Bone Tissue Engineering using 3d Printing. Materials Today 2013;16:496-504.

[24] Helguero CG, Mustahsan VM, Parmar S, Pentyala S, Pfail JL, Kao I, et al. Biomechanical Properties of 3d-Printed Bone Scaffolds are Improved by Treatment with Crfp. J Orthop Surg Res 2017;12:195.

[25] Wieding J, Fritsche A, Heinl P, Körner C, Cornelsen M, Seitz H, et al. Biomechanical Behavior of Bone Scaffolds Made of Additive Manufactured Tricalciumphosphate and Titanium Alloy Under Different Loading Conditions. J Appl Biomater Funct Mater 2013;11:e159-66.

[26] Jariwala SH, Lewis GS, Bushman ZJ, Adair JH, Donahue HJ. 3D Printing of Personalized Artificial Bone Scaffolds. 3D Print Addit Manuf 2015;2:56-64.

[27] Konopnicki S, Sharaf B, Resnick C, Patenaude A, Pogal-Sussman T, Hwang KG, et al. Tissue-engineered Bone with 3-Dimensionally Printed β-tricalcium Phosphate and Polycaprolactone Scaffolds and Early Implantation: An In Vivo Pilot Study in a Porcine Mandible Model. J Oral Maxillofac Surg 2015;73:1016.e1-11.

[28] Yoshimoto H, Shin YM, Terai H, Vacanti JP. A Biodegradable Nanofiber Scaffold by Electrospinning and Its Potential for Bone Tissue Engineering. Biomaterials 2003;24:2077-82.

[29] Hutmacher DW, Schantz T, Zein I, Ng KW, Teoh SH, Tan KC. Mechanical Properties and Cell Cultural Response of Polycaprolactone Scaffolds Designed and Fabricated Via Fused Deposition Modeling. J Biomed Mater Res 2001;55:203-16.

[30] Kim J, McBride S, Tellis B, Alvarez-Urena P, Song YH, Dean DD, et al. Rapid-Prototyped PLGA/β-TCP/Hydroxyapatite Nanocomposite Scaffolds in a Rabbit Femoral Defect Model. Biofabrication 2012;4:025003.

[31] Gunatillake PA, Adhikari R. Biodegradable Synthetic Polymers for Tissue Engineering. Eur Cell Mater 2003; 5:1-16.

[32] Helguero CG, Amaya JL, Ramirez EA, Komatsu DE, Kao I, Pentyala S. A Manufacturing Approach to Functional Biomimetic Three-dimensional-printed Bone implants. Proc Inst Mech Eng Part L J Mater Des Appl 2019;233:383-92.

[33] Mustahsan VM, Anugu A, Komatsu DE, Kao I, Pentyala S. Biocompatible Customized 3D Bone Scaffolds Treated with CRFP, an Osteogenic Peptide. Bioengineering (Basel) 2021;8:199.

[34] Stratasys Technical Report: Biocompatible Clear Med610 Material Data Sheet. 2018. https://www.stratasys.com/siteassets/materials/materials-catalog/biocompatible/mds_pj_med610_0720a.pdf?v=48e364

[35] Komatsu DE, Hadjiargyrou M, Udin SM, Trasolini NA, Pentyala S. Identification and Characterization of a Synthetic Osteogenic Peptide. Calcif Tissue Int 2015;97:611-23.

[36] Orcel P, Tajima H, Murayama Y, Fujita T, Krane SM, Ogata E, et al. Multiple Domains Interacting with Gs in the Porcine Calcitonin Receptor. Mol Endocrinol 2000;14: 170-82.

[37] McGovern JA, Griffin M, Hutmacher DW. Animal Models for Bone Tissue Engineering and Modelling Disease. Dis Model Mech 2018;11:dmm.033084.

[38] Ben-David D, Kizhner T, Livne E, Srouji S. A Tissue-like Construct of Human Bone Marrow MSCs Composite Scaffold Support In Vivo ectopic bone formation. J Tissue Eng Regen Med 2010;4:30-7.

[39] Le Nihouannen D, Daculsi G, Saffarzadeh A, Gauthier O, Delplace S, Pilet P, et al. Ectopic Bone Formation by Microporous Calcium Phosphate Ceramic Particles in Sheep Muscles. Bone 2005;36:1086-93.

[40] Yao J, Li X, Bao C, Zhang C, Chen Z, Fan H, et al. Ectopic Bone Formation in Adipose-Derived Stromal Cell-seeded Osteoinductive Calcium Phosphate Scaffolds. J Biomater Appl 2010;24:607-24.

[41] Qu D, Li J, Li Y, Khadka A, Zuo Y, Wang H, et al. Ectopic Osteochondral Formation of Biomimetic Porous PVA-n-HA/PA6 Bilayered Scaffold and BMSCs Construct in Rabbit. J Biomed Mater Res B Appl Biomater 2011;96: 9-15.

[42] Scott MA, Levi B, Askarinam A, Nguyen A, Rackohn T, Ting K, et al. Brief Review of Models of Ectopic Bone Formation. Stem Cells Dev 2012;21:655-67.

[43] Asatrian G, Chang L, James AW. Muscle Pouch Implantation: An Ectopic bone Formation Model. Methods Mol Biol 2014;1213:185-91.

[44] Wang D, Christensen K, Chawla K, Xiao G, Krebsbach PH, Franceschi RT. Isolation and Characterization of MC3T3-E1 Preosteoblast Subclones with distinct In Vitro and In Vivo Differentiation/Mineralization Potential. J Bone Miner Res 1999;14:893-903.

[45] Tenenbaum HC, Torontali M, Sukhu B. Effects of Bisphosphonates and Inorganic Pyrophosphate on Osteogenesis In Vitro. Bone 1992;13:249-55.

[46] Franceschi RT, Iyer BS, Cui Y. Effects of Ascorbic Acid on Collagen Matrix Formation and Osteoblast Differentiation in Murine MC3T3-E1 Cells. J Bone Miner Res 1994;9: 843-54.

[47] ISO 604: 2002, Plastics-determination of Compressive Properties. Switzerland: International Organization of

Standardization; 2002

[48] Udroiu R, Braga IC. Polyjet Technology Applications for Rapid Tooling. MATEC Web Conf 2017;112:03011.

[49] Chacón J, Caminero MA, García-Plaza E, Núnez PJ. Additive Manufacturing of Pla Structures using Fused Deposition Modelling: Effect of Process Parameters on Mechanical Properties and their Optimal Selection. Mater Design 2017;124:143-57.

[50] DeLustro F, Dasch J, Keefe J, Ellingsworth L. Immune Responses to Allogeneic and Xenogeneic Implants of Collagen and Collagen Derivatives. Clin Orthop Relat Res 1990;260:263-79.

[51] Hasegawa T, Miwa M, Sakai Y, Niikura T, Lee SY, Oe K, *et al*. Efficient Cell-seeding into Scaffolds Improves Bone Formation. J Dent Res 2010;89:854-9.

[52] Polo-Corrales L, Latorre-Esteves M, Ramirez-Vick JE. Scaffold Design for Bone Regeneration. J Nanosci Nanotechnol 2014;14:15-56.

[53] Chen YW, Fang HY, Shie MY, Shen YF. The Mussel-inspired Assisted Apatite Mineralized on PolyJet Material for Artificial Bone Scaffold. Int J Bioprint 2019; 5:197.

[54] Amirrah IN, Lokanathan Y, Zulkiflee I, Wee MF, Motta A, Fauzi MB. A Comprehensive Review on Collagen Type I Development of Biomaterials for Tissue Engineering: From Biosynthesis to Bioscaffold. Biomedicines 2022l;10:2307.

[55] Vepari C, Kaplan DL. Silk as a Biomaterial. Prog Polym Sci 2007;32:991-1007.

[56] Ding Z, Cheng W, Mia MS, Lu Q. Silk Biomaterials for Bone Tissue Engineering. Macromol Biosci 2021;21:e2100153.

[57] Sahoo DR, Biswal T. Alginate and its Application to Tissue Engineering. SN Appl Sci 2021;3:30.

[58] Ressler A. Chitosan-Based Biomaterials for Bone Tissue Engineering Applications: A Short Review. Polymers (Basel) 2022;14:3430.

[59] Kozusko SD, Riccio C, Goulart M, Bumgardner J, Jing XL, Konofaos P. Chitosan as a Bone Scaffold Biomaterial. J Craniofac Surg 2018;29:1788-93.

[60] Collins MN, Ren G, Young K, Pina S, Reis RL, Oliveira JM. Scaffold Fabrication Technologies and Structure/Function Properties in Bone Tissue Engineering. Adv Funct Mater 2021;31:2010609.

[61] Engelberg I, Kohn J. Physico-mechanical Properties of Degradable Polymers used in Medical Applications: A Comparative Study. Biomaterials 1991;12:292-304.

[62] Cheung HY, Lau KT, Lu TP, Hui D. A Critical Review on Polymer-Based Bio-engineered Materials for Scaffold Development. Compos Part B Eng 2006;38:291-300.

[63] Rho JY, Kuhn-Spearing L, Zioupos P. Mechanical Properties and the Hierarchical Structure of Bone. Med Eng Phys 1998;20:92-102.

[64] Ginebra MP, Espanol M, Maazouz Y, Bergez V, Pastorino D. Bioceramics and Bone Healing. EFORT Open Rev 2018;3:173-83.

[65] Bohner M, Santoni BL, Döbelin N. β-Tricalcium Phosphate for Bone Substitution: Synthesis and Properties. Acta Biomater 2020;113:23-41.

[66] Kahar NN, Ahmad N, Mariatti M, Yahaya BH, Sulaiman AR, Hamid ZA. A review of Bioceramics Scaffolds for Bone Defects in Different Types of Animal Models: HA and β -TCP. Biomed Phys Eng Express 2022;8.

[67] Han Q, Wang C, Chen H, Zhao X, Wang J. Porous Tantalum and Titanium in Orthopedics: A Review. ACS Biomater Sci Eng 2019;5:5798-824.

[68] Huang G, Pan ST, Qiu JX. The Clinical Application of Porous Tantalum and its New Development for Bone Tissue Engineering. Materials (Basel) 2021;14:2647.

[69] Crovace AM, Lacitignola L, Forleo DM, Staffieri F, Francioso E, Di Meo A, *et al*. 3D Biomimetic Porous Titanium (Ti6Al4V ELI) Scaffolds for Large Bone Critical Defect Reconstruction: An Experimental Study in Sheep. Animals (Basel) 2020;10:1389.

[70] Qu H, Fu H, Han Z, Sun Y. Biomaterials for Bone Tissue Engineering Scaffolds: A Review. RSC Adv 2019;9:26252-62.

[71] Alizadeh-Osgouei M, Li Y, Wen C. A Comprehensive Review of Biodegradable synthetic polymer-ceramic composites and their Manufacture for Biomedical Applications. Bioact Mater 2018;4:22-36.

[72] Ferreira FV, Otoni CG, Lopes JH, de Souza LP, Mei LH, Lona LM, *et al*. Ultrathin Polymer Fibers Hybridized with Bioactive Ceramics: A Review on Fundamental Pathways of Electrospinning Towards Bone Regeneration. Mater Sci Eng C Mater Biol Appl 2021;123:111853.

[73] George SM, Nayak C, Singh I, Balani K. Multifunctional Hydroxyapatite Composites for Orthopedic Applications: A Review. ACS Biomater Sci Eng 2022;8:3162-86.

[74] Kołodziejska B, Kaflak A, Kolmas J. Biologically Inspired Collagen/Apatite Composite Biomaterials for Potential Use in Bone Tissue Regeneration-A Review. Materials 2020;13:1748.

[75] Schulze F, Lang A, Schoon J, Wassilew GI, Reichert J. Scaffold Guided Bone Regeneration for the Treatment of Large Segmental Defects in Long Bones. Biomedicines 2023;11:325.

Publisher's note

AccScience Publishing remains neutral with regard to jurisdictional claims in published maps and institutional affiliations.